



Realization of a Stabilized Carbon Dioxide Laser System at the BIPM

Part 1: Construction of the Carbon Dioxide Laser

Susanne Picard

Bureau International des Poids et Mesures
Pavillon de Breteuil
92312 Sèvres Cedex France

Realization of a Stabilized Carbon Dioxide Laser System at the BIPM

Part 1: Construction of the Carbon Dioxide Laser

Susanne Picard

Bureau International des Poids et Mesures
Pavillon de Breteuil
92312 Sèvres Cedex France

Abstract

A CO₂ laser constructed at the BIPM is described.

Part 1: Construction of the Carbon Dioxide Laser

Table of Contents

1 Introduction	5
2 The CO ₂ Molecule as a Laser Medium	6
3 Description of the Laser System	12
3.1 Laser Tube	12
3.2 Optics	15
3.3 Laser Support and Mechanics	16
3.4 Pump System	18
3.5 Power Supply	19
4 Installation	20
4.1 Cleaning and Running	20
4.2 Alignment	20
4.3 Pumping	20
4.4 Running	21
4.5 Maintenance	21
5 First Results from the Unstabilized Laser	22
5.1 Choice of Modulation Frequency	22
5.2 Beam Characteristics	23
5.2.1 Descriptive Laser Parameters	23
5.2.1.1 Formulas	23
5.2.1.2 Parameters of the BIPM CO ₂ Laser	25
5.2.2 Beam Profile	25
5.2.3 Pressure and Intensity	28
5.3 First Comparison	28
Acknowledgement	31
References	31

1 Introduction

Carbon dioxide laser radiation was first observed in the early sixties as a result of the successful work by Patel [1] and the group of Legay-Sommaire [2]. Since then, this light source which is able to create high-power infra-red radiation, has been used in numerous applications in medicine, manufacturing industry, environmental studies and military activities. It is also frequently used in molecular spectroscopy.

Of particular interest in the seventies was the potential use of the CO₂ laser as a frequency standard. Extensive research by Bordé and his colleagues on saturation spectroscopy of OsO₄, SF₆ and other poly-atomic molecules (see for example [3]) was a major contribution to the progress of stabilized CO₂ laser systems. Nowadays, high accuracy stabilized CO₂ lasers exist in several laboratories around the world. Some are used as absolute frequency standards, providing a frequency precision of 50 Hz [4,5]. This result has been obtained by measuring the absorbed frequency with a frequency chain using a caesium clock to provide the fundamental frequency. A stabilized CO₂ laser system has recently been used to determine the absolute frequency of red He-Ne 633nm laser radiation [6].

Following a decision to extend our activity of the length section of the BIPM to include CO₂ lasers, our project began by spending a month in the laboratories at Laboratoire Primaire du Temps et des Fréquences (LPTF) to become acquainted with the experimental setup by André Clairon and Ouali Acef. A visit was also made to Christian Bréant at the Etablissement Technique Central de l'Armement (ETCA).

The purpose of this report, Part I, is to describe the first CO₂ laser at the BIPM and explain how it functions. A detailed description of the lasers at the LPTF was presented in the thesis by Ouali Acef [7], and the lasers at ETCA have been described in an internal report of the ETCA [8]. In Part II of this report a Fabry-Perot interferometer which is used for frequency discrimination will be described. In Part III the stabilized laser system will be presented.

2 The CO₂ Molecule as a Laser Medium

In contrast to diatomic molecules that vibrate only along their internuclear axis [9], triatomic molecules have a more complicated vibrational pattern. However, the vibration of a linear triatomic molecule can be looked upon as a superposition of three different modes of vibration: symmetric stretching (ν_1), bending (ν_2) and asymmetric stretching (ν_3). These three modes are represented in Fig.1. In order to represent a specific vibrational state, one uses the notation ($\nu_1 \nu_2^l \nu_3$). As the molecule can bend in two perpendicular planes, creating two degenerate vibrational modes, a suffix "1" is added to ν_2 .

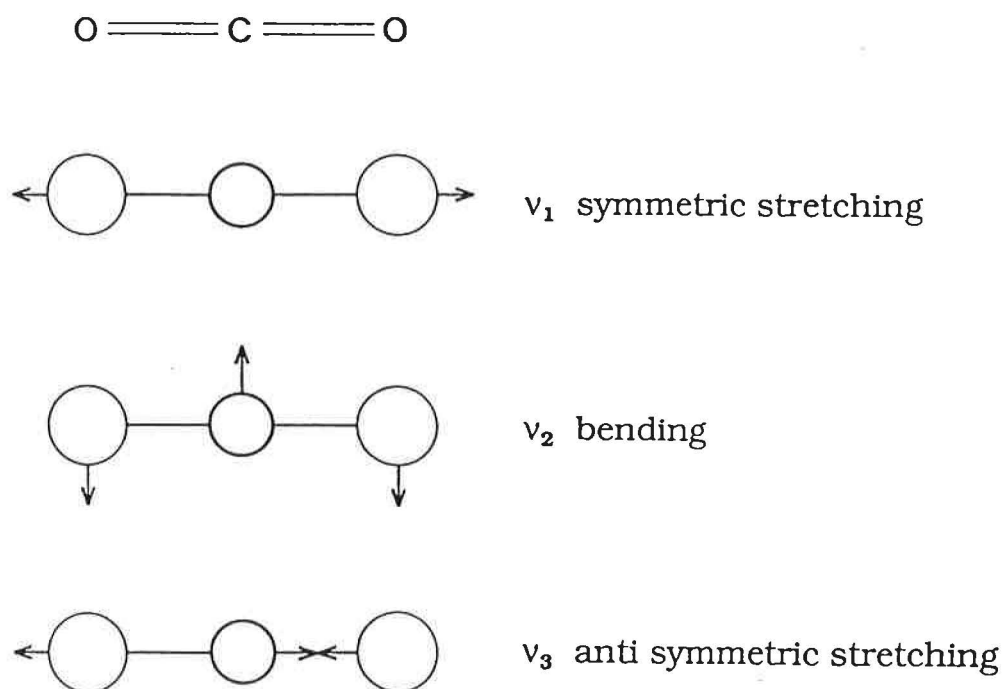


Fig.1. Schematic representation of the three vibrational modes ν_1 , ν_2 and ν_3 for a linear triatomic molecule, like CO₂.

The first mode of vibration, ν_1 , is symmetric and can be represented by Σ^+_g symmetry [10]. The ν_3 vibration is anti-symmetric and is represented by Σ^+_u . The bending modes are represented by Π_u . We know that there are well established selection rules [11],

$$g \leftrightarrow u \quad (1-a)$$

$$+ \leftrightarrow - \quad (1-b)$$

$$s \not\leftrightarrow a \quad (1-c)$$

$$\Delta J = \pm 1, 0, \quad (1-d)$$

where g and u represent gerade and ungerade, + and - represent positive and negative parity, and s and a represent symmetric and anti-symmetric levels respectively. Apart from the molecular vibration, the molecule can also rotate. The rotational quantum number is represented by J. The difference between the upper rotational quantum number J' and the lower one, J'' , is given by ΔJ .

The carbon dioxide molecule, CO_2 , is a linear triatomic molecule having central symmetry. A simplified scheme for the lowest vibrational levels of the electronic ground state of CO_2 is shown in Fig.2. The rotational levels are not indicated. Two bands of laser transitions are possible, marked by solid lines, of which the $(00^0_1)-(10^0_0)$ is the strongest and corresponds to the well-known $10,6 \mu\text{m}$ infrared radiation. In the figure, the symmetric states are also indicated. As can be seen, the (02^0_0) bending state is a Σ^+_g state and not a Π_u state. This results from a perturbation, referred to as a Fermi resonance [10].

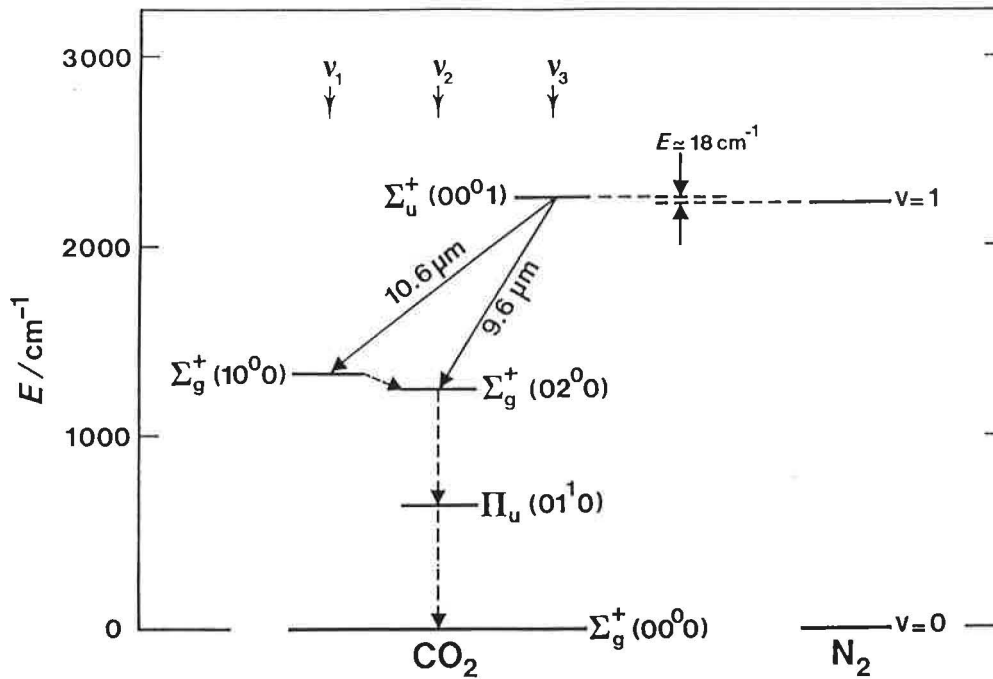


Fig.2. Simplified scheme for the lowest vibrational levels of the electronic ground state of CO_2 . The three different modes of vibration are shown in the top of the figure. The rotational levels are not indicated. The two possible bands of laser transitions are marked with solid lines. The collisional resonance of the N_2 molecule is shown in schematic form on the right.

Figure 3 represents the transition scheme between the upper and lower state in the 10,6 μm transition, $(00^01)-(10^00)$, or a $\Sigma^+_{\text{u}}-\Sigma^+_{\text{g}}$ transition. The symmetry, parity and rotational quantum numbers are indicated. In the most abundant form of CO_2 , $^{16}\text{O}=^{12}\text{C}=^{16}\text{O}$, the nuclear spin $I=0$. For symmetry reasons, only the s-levels are populated. The s-levels are indicated by thick lines, and the unpopulated a-levels by thin lines. For a $\Sigma - \Sigma$ transition only $\Delta J = \pm 1$ lines are allowed. Therefore, as indicated in the figure, only R ($\Delta J = +1$) and P ($\Delta J = -1$) lines are observable, and all transitions with odd J'' numbers are absent, due to the nuclear spin. In Table 1 an extract from Bradley et al. [12] is listed, giving the calculated frequencies and wavenumbers for some of the R and P lines in $^{12}\text{C}^{16}\text{O}_2$.

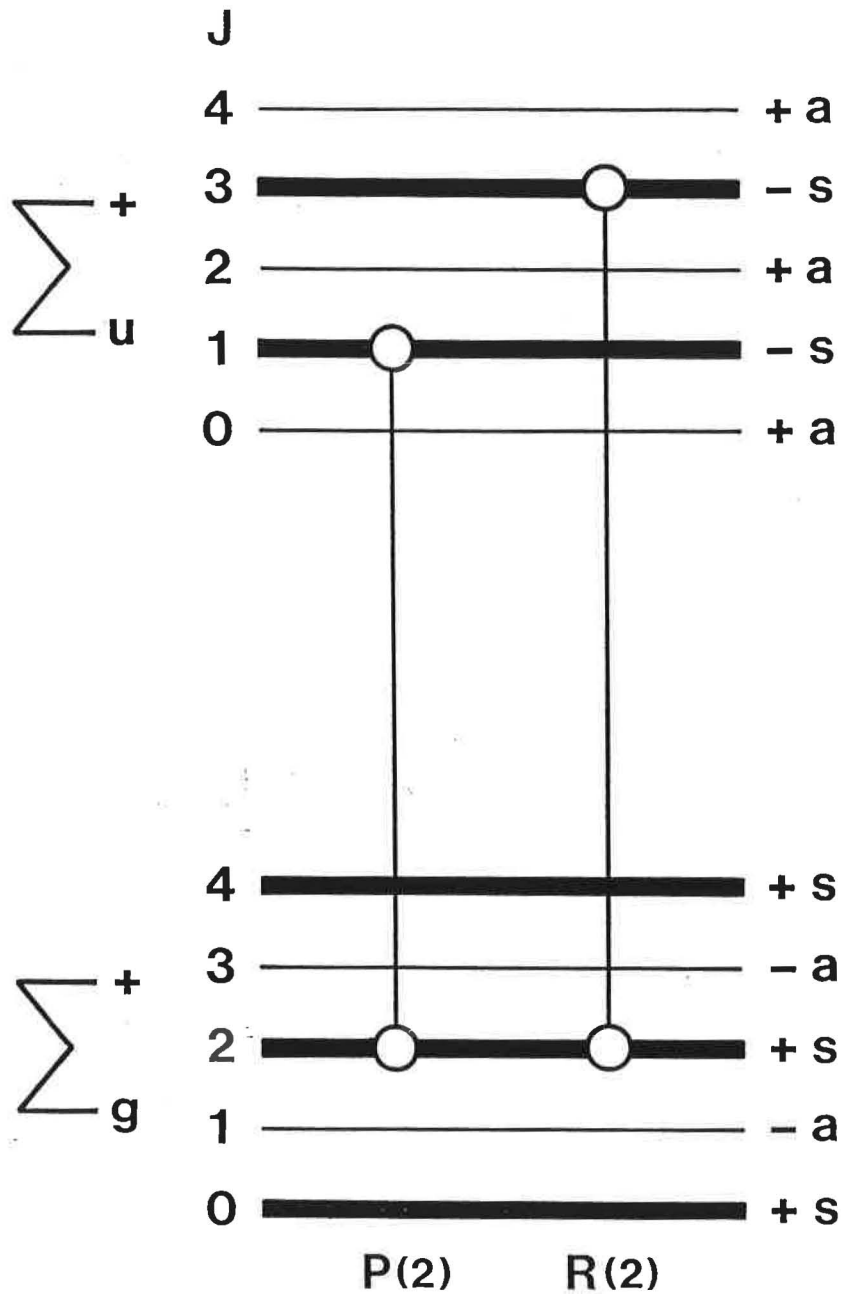
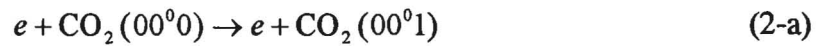


Fig.3. Transition scheme between the upper and lower state in the 10,6 μm transition. The symmetry, parity and rotational quantum numbers are indicated. Due to the nuclear spin ($I=0$) and for symmetry reasons only s-levels are populated, represented by thick lines. Hence, only R and P lines are observable, and all transitions with odd J'' numbers are absent.

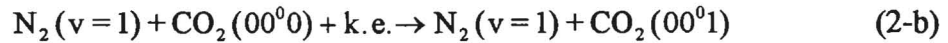
BAND I				BAND II			
LINE	FREQUENCY (MHZ)	STD. DEV. (MHZ)	VAC. WAVE NO. (CM-1)	LINE	FREQUENCY (MHZ)	STD. DEV. (MHZ)	VAC. WAVE NO. (CM-1)
P(60)	2707 7607.5077	0.0246	903.2117 6484	P(60)	3014 3456.0742	0.0172	1005.4774 6515
P(58)	2714 6404.4578	0.0154	905.5065 8408	P(58)	3021 2223.6949	0.0110	1007.7713 0607
P(56)	2721 4396.1809	0.0097	907.7745 4384	P(56)	3028 0322.1201	0.0072	1010.0428 2503
P(54)	2728 1588.8741	0.0064	910.0158 5084	P(54)	3034 7743.7465	0.0051	1012.2917 6841
P(52)	2734 7988.4259	0.0049	912.2307 0148	P(52)	3041 4481.1364	0.0042	1014.5178 8812
P(50)	2741 3600.4235	0.0043	914.4192 8214	P(50)	3048 0527.0251	0.0039	1016.7209 4183
P(48)	2747 8430.1601	0.0040	916.5817 6938	P(48)	3054 5874.3277	0.0038	1018.9006 9322
P(46)	2754 2482.6413	0.0038	918.7183 3017	P(46)	3061 0516.1462	0.0039	1021.0569 1219
P(44)	2760 5762.5914	0.0037	920.8291 2210	P(44)	3067 4445.7759	0.0039	1023.1893 7509
P(42)	2766 8274.4599	0.0036	922.9142 9359	P(42)	3073 7656.7119	0.0039	1025.2978 6496
P(40)	2773 0022.4271	0.0036	924.9739 8407	P(40)	3080 0142.6555	0.0039	1027.3821 7169
P(38)	2779 1010.4094	0.0036	927.0083 2419	P(38)	3086 1897.5199	0.0038	1029.4420 9223
P(36)	2785 1242.0651	0.0035	929.0174 3596	P(36)	3092 2915.4360	0.0038	1031.4774 3083
P(34)	2791 0720.7986	0.0035	931.0014 3295	P(34)	3098 3190.7583	0.0038	1033.4879 9917
P(32)	2796 9449.7656	0.0035	932.9604 2043	P(32)	3104 2718.0700	0.0038	1035.4736 1655
P(30)	2802 7431.8776	0.0035	934.8944 9550	P(30)	3110 1492.1877	0.0037	1037.4341 1009
P(28)	2808 4669.8055	0.0035	936.8037 4726	P(28)	3115 9508.1671	0.0037	1039.3693 1486
P(26)	2814 1165.9839	0.0035	938.6882 5692	P(26)	3121 6761.3064	0.0037	1041.2790 7402
P(24)	2819 6922.6147	0.0036	940.5480 9793	P(24)	3127 3247.1518	0.0038	1043.1632 3901
P(22)	2825 1941.6703	0.0036	942.3833 3608	P(22)	3132 8961.5006	0.0038	1045.0216 6964
P(20)	2830 6224.8967	0.0036	944.1940 2961	P(20)	3138 3900.4054	0.0038	1046.8542 3425
P(18)	2835 9773.8165	0.0036	945.9802 2931	P(18)	3143 8060.1774	0.0037	1048.6608 0978
P(16)	2841 2589.7314	0.0035	947.7419 7860	P(16)	3149 1437.3897	0.0037	1050.4412 8194
P(14)	2846 4673.7246	0.0035	949.4793 1361	P(14)	3154 4028.8804	0.0037	1052.1955 4524
P(12)	2851 6026.6628	0.0035	951.1922 6324	P(12)	3159 5831.7547	0.0037	1053.9235 0313
P(10)	2856 6649.1983	0.0035	952.8808 4927	P(10)	3164 6843.3878	0.0037	1055.6250 6805
P(8)	2861 6541.7701	0.0035	954.5450 8632	P(8)	3169 7061.4264	0.0037	1057.3001 6151
P(6)	2866 5704.6061	0.0036	956.1849 8202	P(6)	3174 6483.7910	0.0037	1058.9487 1415
P(4)	2871 4137.7235	0.0036	957.8005 3691	P(4)	3179 5108.6771	0.0037	1060.5706 6576
P(2)	2876 1840.9300	0.0036	959.3917 4460	P(2)	3184 2934.5560	0.0037	1062.1659 6536
V(0)	2880 8813.8246	0.0036	960.9585 9171	V(0)	3188 9960.1764	0.0037	1063.7345 7121
R(0)	2883 2026.2225	0.0036	961.7328 7396	R(0)	3191 3172.5743	0.0037	1064.5088 5347
R(2)	2887 7902.4412	0.0036	963.2631 3990	R(2)	3195 8996.0672	0.0036	1066.0373 6066
R(4)	2892 3046.4336	0.0036	964.7689 8140	R(4)	3200 4017.3872	0.0036	1067.5391 1025
R(6)	2896 7457.0695	0.0035	966.2503 6076	R(6)	3204 8236.2544	0.0036	1069.0140 9289
R(8)	2901 1133.0097	0.0035	967.7072 3331	R(8)	3209 1652.6660	0.0036	1070.4623 0849
R(10)	2905 4072.7058	0.0035	969.1395 4739	R(10)	3213 4266.8953	0.0036	1071.8837 6618
R(12)	2909 6274.3988	0.0034	970.5472 4435	R(12)	3217 6079.4907	0.0036	1073.2784 8423
R(14)	2913 7736.1185	0.0034	971.9302 5845	R(14)	3221 7091.2743	0.0037	1074.6464 9008
R(16)	2917 8455.6817	0.0033	973.2885 1688	R(16)	3225 7303.3400	0.0037	1075.9878 2021
R(18)	2921 8430.6909	0.0033	974.6219 3965	R(18)	3229 6717.0518	0.0037	1077.3025 2013
R(20)	2925 7658.5324	0.0032	975.9304 3960	R(20)	3233 5334.0411	0.0038	1078.5906 4423
R(22)	2929 6136.3740	0.0032	977.2139 2224	R(22)	3237 3156.2043	0.0039	1079.8522 5580
R(24)	2933 3861.1629	0.0032	978.4722 8575	R(24)	3241 0185.7000	0.0039	1081.0874 2682
R(26)	2937 0829.6231	0.0031	979.7054 2084	R(26)	3244 6424.9456	0.0039	1082.2962 3794
R(28)	2940 7038.2525	0.0031	980.9132 1071	R(28)	3248 1876.6140	0.0040	1083.4787 7831
R(30)	2944 2483.3197	0.0031	982.0955 3089	R(30)	3251 6543.6298	0.0040	1084.6351 4549
R(32)	2947 7160.8609	0.0031	983.2522 4916	R(32)	3255 0429.1653	0.0039	1085.7654 4528
R(34)	2951 1066.6762	0.0031	984.3832 2542	R(34)	3258 3536.6360	0.0039	1086.8697 9163

Tab. 1. Extract from Bradley et al. [12], listing the calculated frequencies and wavenumbers for some of the R and P branches in $^{12}\text{C}^{16}\text{O}_2$.

Two main processes are responsible for the laser excitation: i) excitation through electron collision in CO₂, created by a high voltage discharge, which can be written



and ii) excitation by collisions where the kinetic energy, k.e., is transferred from N₂ to CO₂ which can be written



(The N₂ molecule excited to v=1 in its electronic ground state differs by only 18 cm⁻¹ from the upper (00⁰¹) level of CO₂.) This is the same principle of excitation as for the He-Ne laser and is schematised on the right of Fig.2.

The lower laser levels, (10⁰⁰) and (20⁰⁰) both relax into the (01¹⁰) level. The relaxation pathways are marked with broken lines in Fig.2. Laser action is possible when the (01¹⁰) level has a shorter lifetime than the upper laser level. This is not the case in pure CO₂, but the problem can be overcome by adding He which accelerates the relaxation process of the (01¹⁰) level. Additionally, the He provides important heat transfer to the walls of the laser (which can be cooled externally), since it is known that the laser gain and laser power decrease with increasing temperature [13].

It may be concluded that an efficient CO₂ laser also contains N₂ and He. Sometimes H₂O or H₂ are added to favour the recombination processes that follow the dissociation induced by the discharge. The role of these molecules is however a matter for discussion.

3 Description of the Laser System

The laser system is described in five parts:

- 1) laser tube
- 2) optics
- 3) laser support and mechanics
- 4) pump system
- 5) power supply

3.1 Laser Tube

The laser glass tube was constructed using tubes of LPTF design as prototypes [7,14,15]. Only a few modifications were made, of which some ideas originate from the ETCA realization [8]. The tube was constructed by a glass blowing company near Paris.

The laser that has been constructed is of sealed type¹ i.e. no gas is added or taken away when the laser is running. However, the laser contains a buffer gas cavity. During discharge, small pressure changes are induced which create a slow gas flow into or out of the buffer. This favours recombination of the CO₂ gas mixture.

The laser tube is shown in Fig.4-a. It is 1 m long, made of borosilicate glass with a metal-glass connection leading to a 25 mm long flexible tube connected to a rotatable flange (CF40) at each end. The tube consists of three different glass cavities: i) the inner cavity (Φ 9 mm) through which the radiation passes, ii) the middle cavity (Φ 40 mm) which contains circulating water to cool the laser and iii) the outer cavity (Φ 70 mm), connected to the inner one by a bypass at each end of the tube, used as a gas buffer. The water connections can be screwed on and a small flow is enough (0.3-0.4 l/min) to cool the laser. A glass bellows is placed on each side of the tube, to avoid mechanical stress in the glass caused by thermal expansion.

¹ An instructive review of different types of CO₂ lasers can be found in [16].

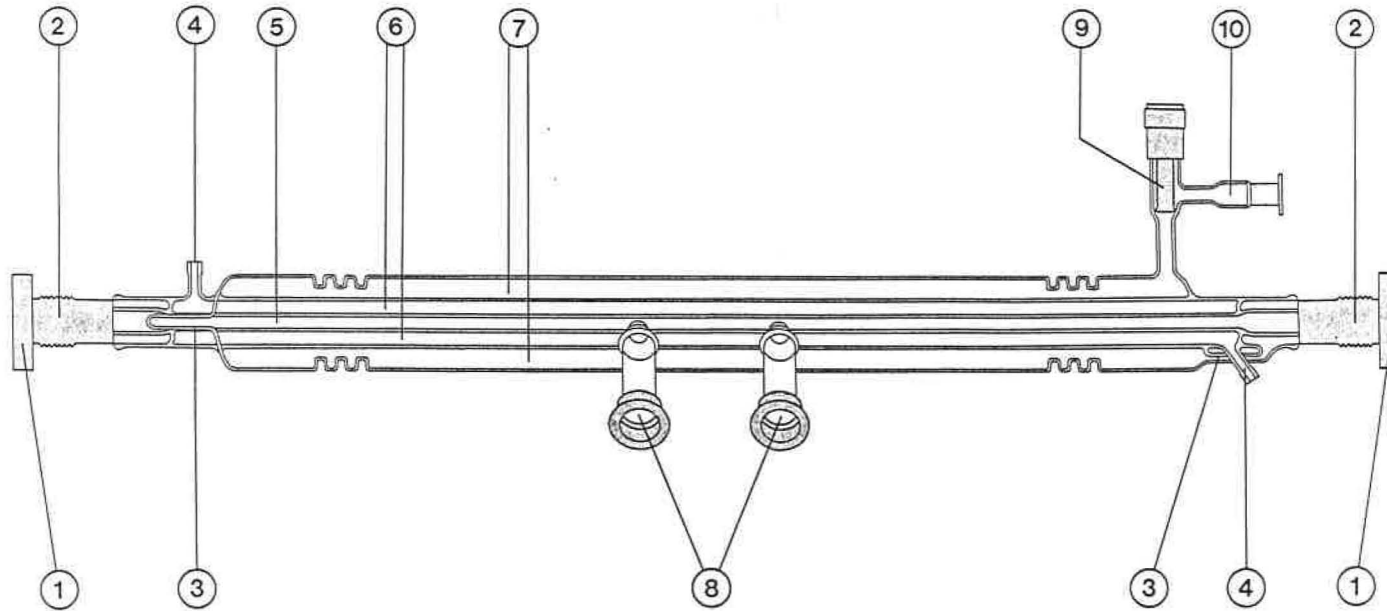


Fig.4-a. Drawing of laser tube seen from the side. The tube measures 1 m between each extremity. 1 - Rotatable CF flange. 2 - Flexible tube. 3 - Bypass for the gas between the inner and outer cavity. 4 - Demountable water connection. 5 - Inner gas cavity. 6 - Water cooling cavity. 7 - Outer gas buffer. 8 - Cathode cavities. 9 - Gas valve. 10 - Gas inlet.

The laser tube is symmetric about the central plane normal to its axis. At each end a circular, threaded anode holder, perforated to speed evacuation of the tube, is soldered close to the metal-glass union, see Fig.4-b. At a distance of 450 mm from each end a glass tube is inclined at 120 degrees to the vertical and terminated with an ISO40 flange, containing a copper electrode. This geometry is chosen so that any particular material formed in the tube does not fall into the reaction region. A gas inlet for the CO₂ is soldered to the gas buffer container at which also the pump system is connected when needed.

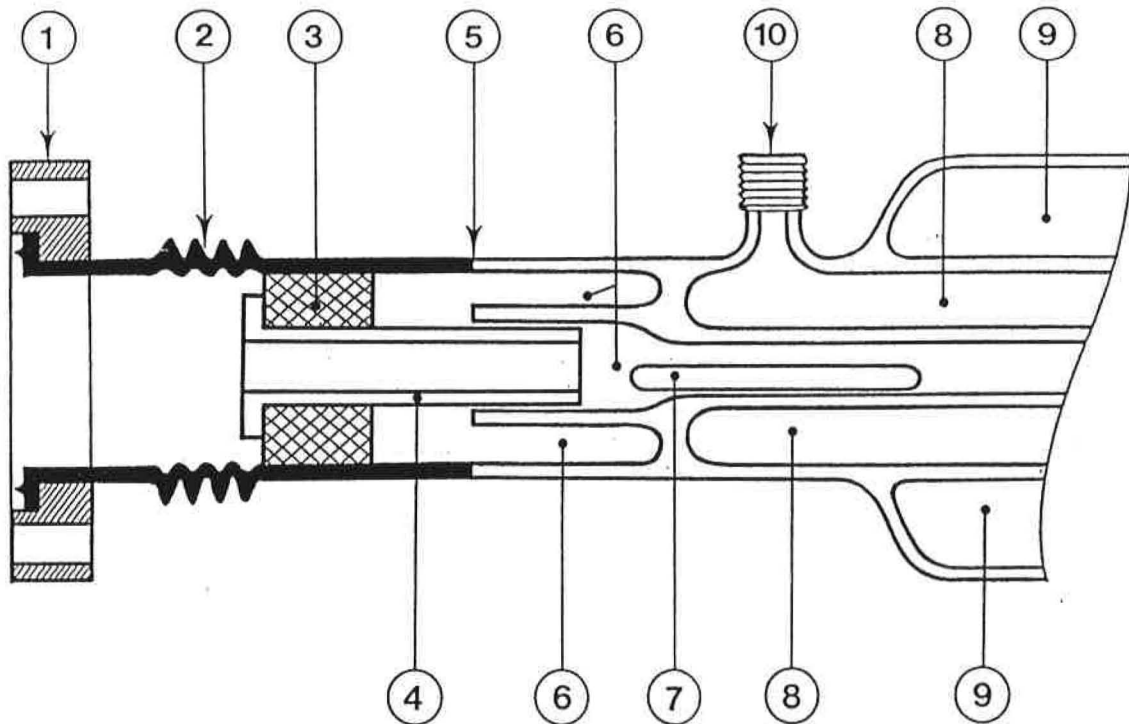


Fig.4-b. Detail of one of the laser extremities. 1 - Rotatable CF flange. 2 - Flexible tube. 3 - Soldered threaded anode holder. 4 - Nickel anode. 5 - Glas-metal connection. 6 - Inner gas cavity. 7 - Bypass for the gas. 8 - Water cooling cavity. 9 - Outer gas buffer. 10 - Demountable water connection.

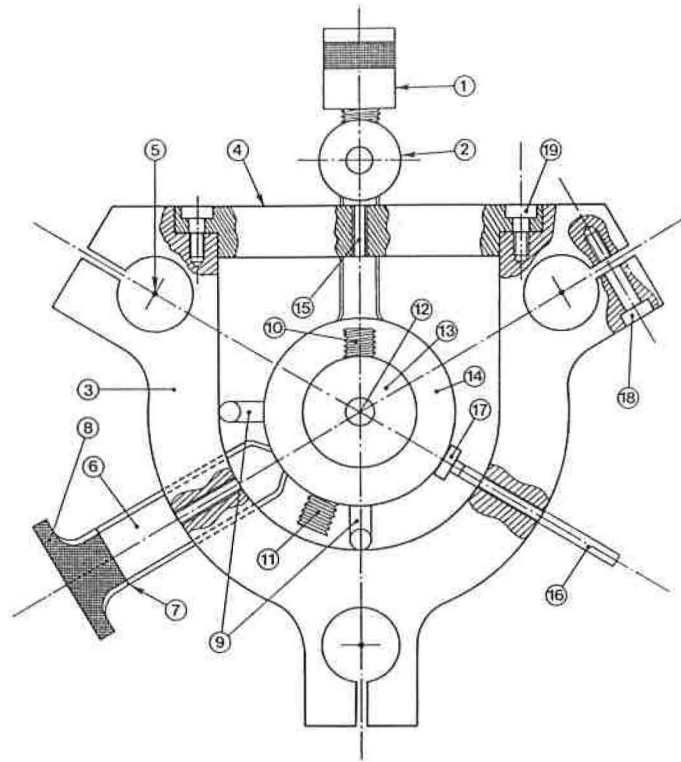


Fig.4-c. Cross section of laser tube mounted in its support. 1 - Valve. 2 - Gas inlet. 3 - Aluminium support. 4 - Dismountable rod. 5 - Hole for invar rods. 6 - Cathode container. 7 - Glas-metal soldering. 8 - ISO-flange. 9 - Bypass for the gas. 10 - Water output. 11 - Water input. 12 - Inner gas cavity. 13 - Water cavity. 14 - Outer gas cavity. 15 - Hole for screws securing the tube. 16 - Teflon ended securing screw. 17 - Teflon cap. 18 - Screw to fix the support to the invar bars. 19 - Screw.

3.2 Optics

For infrared radiation at about $10\ \mu\text{m}$, the choice of transparent optical material is restricted. The most common materials are Si, Ge or ZnSe. The ZnSe is perhaps the most convenient (and most expensive) choice as its transmission band is wide ($0,55\ \mu\text{m} - 16\ \mu\text{m}$). This means that red He-Ne $633\ \text{nm}$ laser light is also transmitted which is useful for alignment. The ZnSe also possesses superior thermal characteristics: it is better, for example, than Ge which becomes opaque when heated. Reflective coatings are mostly of copper, silver or gold.

The laser cavity has one gold coated ZnSe partial reflector ($\Phi\ 25\ \text{mm}$, $R=4\ \text{m}$) with a reflectivity of 95% on one side. The outer side is treated to reduce reflection. The other side of the cavity is fitted with a gold coated grating. Its active surface is $16\ \text{mm} \times 16\ \text{mm}$ with 150 lines/mm. With this grating constant, the strongest P lines in the $10,6\ \mu\text{m}$ transition fall about 50° away from the normal to the surface. Using an incident He-Ne $633\ \text{nm}$ laser beam, the sixteenth order can be observed at about this angle.

3.3 Laser Support and Mechanics

The entire laser support was constructed in the mechanical workshop at the BIPM. It differs from those used at the LPTF and the ETCA. The construction materials are invar, stainless steel and aluminium. Some materials were chosen to avoid sticking. The laser was designed not to be too heavy to facilitate transport.

The support consists of three 1,12 m long invar rods (Φ 28 mm) each made up of four parts which are screwed together. A stainless steel support is placed at each extremity to give rigidity. Five supplementary aluminium supports are arranged equidistant along the rods. Each support is equipped with three teflon coated screws that exert forces on the laser tube; these influence the linearity and laser action slightly.

The rods and supports were initially hung in a flexible support, directly inspired by the design of Raymond Felder (BIPM). Felder has obtained good results with lasers supported in this way [17]. However, this system was later replaced by rigid supports, to ensure a good beam pointing stability. We also added a support for the glass valve of the laser tube, so that it would not break when being attached to the pump system.

The reflecting surface of the end mirror is glued, using an epoxy resin (Techkits E-7), to a 40 mm long piezo-electric cylindrical ceramic tube (Φ 22x18 mm). The ceramic is divided into two parts; one part provides the frequency modulation, the other corrects for the frequency drift. The ceramic itself is glued to a CF flange, isolated by a plexiglass disk. The inside of the cylinder is connected to separate ground through an insulating wire passing through the flange. The arrangement is shown in Fig.4-d. The outside of the cylinder was covered by an insulating layer of epoxy resin and soldered teflon wires are connected to BNC inputs. The whole flange is mounted on a conventional XY-flexible holder, attached to the laser and one of the end supports.

The grating holder is contained in a stainless steel cylinder 92 mm deep (Φ 120 mm), attached to the opposite end support. The grating is inclined at an angle of about 50° to the incident laser beam. It can be moved in two dimensions through two rotatable and flexible rods. The rods turn two large and fine threaded brass screws; one turns the holder about a vertical axis, the other turns the holder about a horizontal axis. The chosen position is maintained in place by rigid springs. A graded scale allows control of the position. The adjustments can be observed through a vacuum window at the end of the steel cylinder.

The laser discharge is maintained between two anode-cathode pairs. The 40 mm long cylindrical hollow cathode (Φ 8 mm) is made in copper. It is mounted on a 40 mm long stainless-steel rod screwed to the end support. The cathodes are placed in individual glass tubes. The anodes are of Ni. Nickel is often chosen as the anode material for CO₂ lasers as it has been shown to have a catalytic effect on the recombination process after the laser discharge. The anodes are cylindrical, 50 mm long (Φ 10 mm) and are screwed into the anode holders using a special key.

Unwanted transverse laser modes are suppressed by an intercavity diaphragm. A small holder, constructed for this purpose, simplifies the manipulation when changing the diameter of the diaphragm. It is placed next to the grating holder.

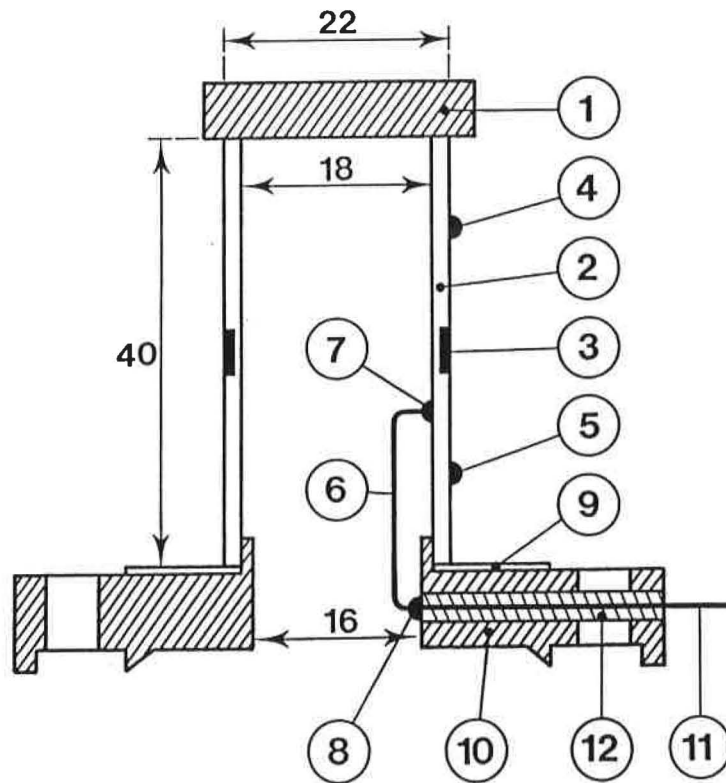


Fig.4-d. Scheme of piezo electric holder. 1 - ZnSe partial reflector. 2 - Piezo electric ceramic. 3 - Insulation. 4 - Frequency modulation connection. 5 - High voltage connection. 6 - Connection for ground separation. 7,8 - Solder. 9 - Plexiglass plate. 10 - Stainless steel flange. 11 - Metal wire. 12 - Glass insulation.

3.4 Pump System

The pumping system is shown schematically in Fig.5 and is mounted on a mobile table, constructed in the mechanical workshop. It comprises a primary pump connected through a liquid nitrogen trap to an air-cooled turbo molecular pump. The pressure is measured by a penning gauge and a capacitance manometer. The CO₂/He/N₂ mixture is connected to the gas inlet through a needle valve.

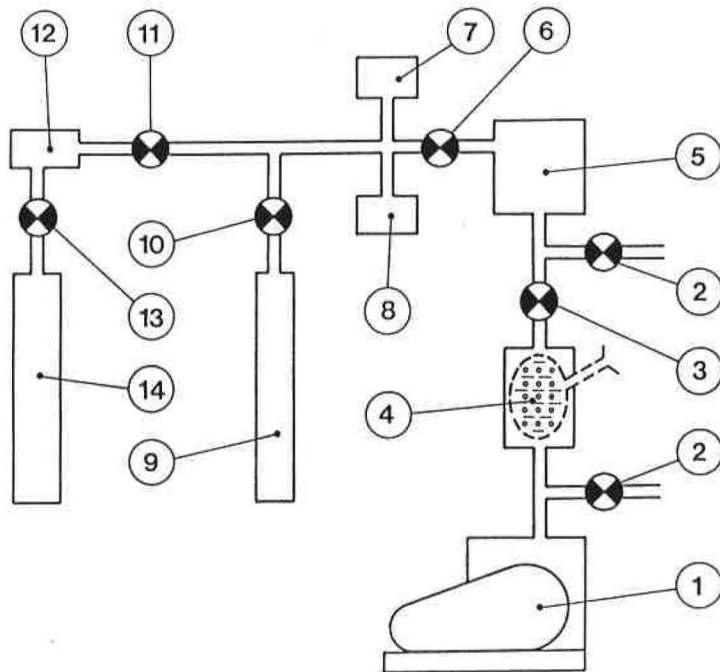


Fig.5. Pump scheme. 1 - Primary pump. 2,3,6,10,11,13 - Valve. 4 - Vacuum trap. 5 - Turbo molecular pump. 7 - Penning manometer. 8 - Capacity manometer. 9 - CO₂ mixture gas tube. 12 - Gas inlet cavity. 14 - Laser cavity.

3.5 Power Supply

A stabilized high voltage power supply (Siemel) is used to create the gas discharge. Its current stability is of the order of one part in 10^6 . It is connected through series coupled $150\text{ k}\Omega$ ballast resistances to the copper cathodes, see Fig.6. The anode was kept at ground, in common with the ground of the laser support.

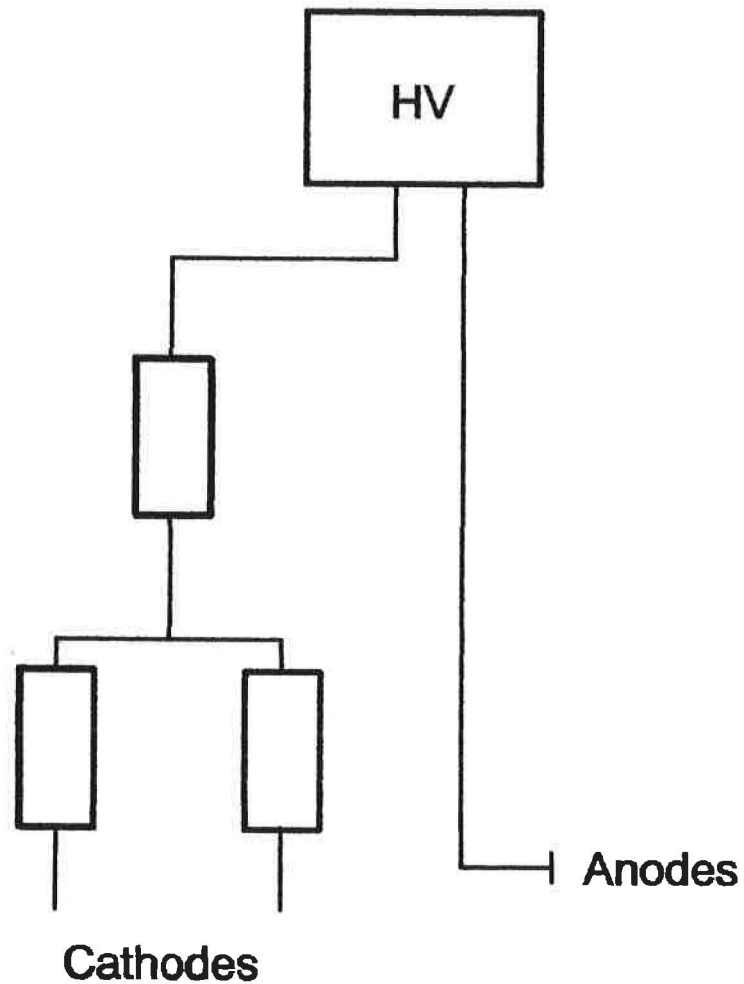


Fig.6. Arrangement of ballast resistance connection.

4 Installation

4.1 Cleaning and Mounting

Before assembling the laser all metal parts were carefully cleaned. They were cleaned twice in tri-chlor-ethylene and once in ethanol, using an ultra sonic cavity. They were then heated to about 40°C in an evacuated oven to accelerate the degassing. This procedure was repeated each time a mechanical modification had to be made. The laser tube itself was initially cleaned twice in ethanol to remove dust particles.

When gluing the piezo electric ceramic onto the mirror and holder, see Sec.3.3, the auto collimation was adjusted with an aligned red He-Ne laser. In this way it was possible to check that the mirror is parallel to the surface of the holder.

The laser was mounted without using grease on the vacuum connections and the inner mechanics. However, after difficulties with sticking screws, vaseline was used to make the movement of the mirror adjuster smoother. Rubber O-rings were used for the diaphragm holder flange, the laser valve and the cathode holder flanges. All other vacuum connections were made using copper seals. Two teflon rings were added, placed around the copper cathodes in order to guide the cathodes. No degassing from these rings was observed.

4.2 Alignment

The alignment of the laser was first done without the front mirror or grating. The linearity of the laser glass tube was first verified using a collimated He-Ne laser beam 7 mm in diameter and it was found to be satisfactory. Next step was to mount the grating. By examining the return beam the grating could be located so that its grooves were parallel to the axis of rotation, and the beam was auto collimated. Finally, keeping the system auto collimated, the mirror was mounted. In this condition, supposing that the two mirror faces are parallel, only a horizontal displacement should be required to initiate laser action.

4.3 Pumping

Before the laser could be used efficiently, it had to be pumped and degassed. The pump system is described in Sec.3.4. The laser was heated to 100 °C with wires wrapped around parts of the laser system. A pressure of about 1×10^{-4} Pa (8×10^{-7} torr) could be obtained after baking and degassing.

4.4 Running

When all mechanical parts were clean and a sufficient vacuum had been obtained, the laser was filled with the CO₂ mixture. This consisted of 13% CO₂, 13% N₂ and 74% He, see Sec.2.1. The tube was first filled to 500 Pa (4 torr). The gas discharge was started with an initial power peak of about 10 kV. The discharge current was then maintained at about 20 mA while continuously filling the tube to 900-1300 Pa (7-10 torr). A faint violet fluorescence could then be observed in the inner laser cavity between each anode and cathode pair.

Laser operation was attempted by keeping the He-Ne laser autocollimated, and changing the alignment slightly. When laser action was identified using either thermo sensitive plastic films, thermo sensitive paper or by detecting the radiation with a power meter, the alignment was optimized. This was done by i) adjusting the laser mirror inclination in x-y-direction, ii) adjusting the grating inclination, and iii) carefully pressing the laser glass tube with the teflon coated side screws, see Fig.4-c. More than 5 W of radiated power at 10,6 μm was obtained at a gas pressure of 1600 Pa (12 torr) by adjusting the alignment. At 1300 Pa (10 torr), more than 3 W of radiated power was achieved on the P(18) line.

The laser beam output turned out to be a transverse multi-mode combination. This could be avoided by reducing the free inner diameter of the laser tube. Different sizes of inter cavity diaphragms were tried, see Sec.3.3. Using a diaphragm of 6 mm diameter a laser output up to 1,5 W on the P(18) line could be obtained when the laser cavity length was tuned. The intensity profile then became less complicated. This is discussed in detail in Sec.5.

4.5 Maintenance

The cathodes are oxidized by use and have to be cleaned regularly. The cleaning procedure proposed by LPTF [15] was used: the inner and outer surface of the cathodes were first polished with the finest grade of glass paper and then cleaned in an ultra-sonic bath containing tri-chlor-acetylene. They were then put in an acid bath containing 90% orthophosphoric acid, 5% nitric acid and 5% acetic acid for a few minutes. After carefully cleaning them in an ultra sonic bath containing distilled water, they are finally rinsed in an ultrasonic bath containing ethanol.

The laser has to be refilled with gas after about six weeks.

5 First Results from the Unstabilized Laser

5.1 Choice of Modulation Frequency

To ensure that the piezo electric ceramic (pzt) has no resonance at the chosen modulation frequency, the spectrum of the laser output was studied as a function of modulation frequency using the HgCdTe detector and a spectrum analyser. Figure 7-a shows a typical spectrum when the pzt is in resonance with the modulation frequency; several harmonics can be found around the central frequency (marked with a white dot). Figure 7-b shows the output signal when no observable resonance is present. This criteria is essential for the use of third harmonic locking technique. Modulation frequency at 2,8 kHz was found to be suitable.

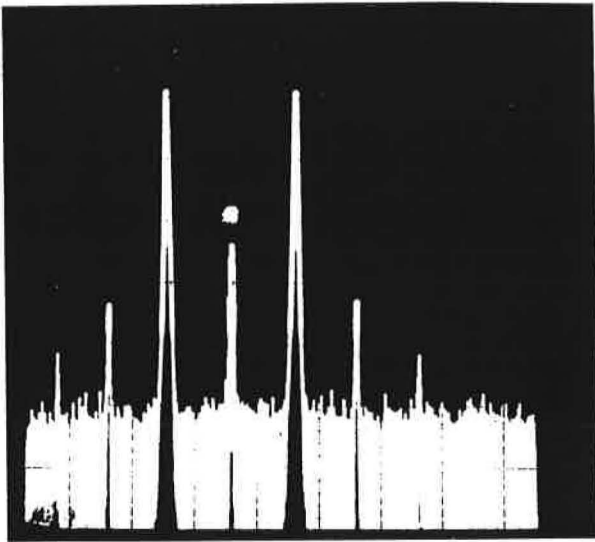


Fig.7-a. Photograph of spectrum analyser screen with 10 kHz/div. The modulation frequency was set to 10.4 kHz, which is one of the resonances of the pzt, giving multiple harmonics. The center frequency is indicated with a white dot.

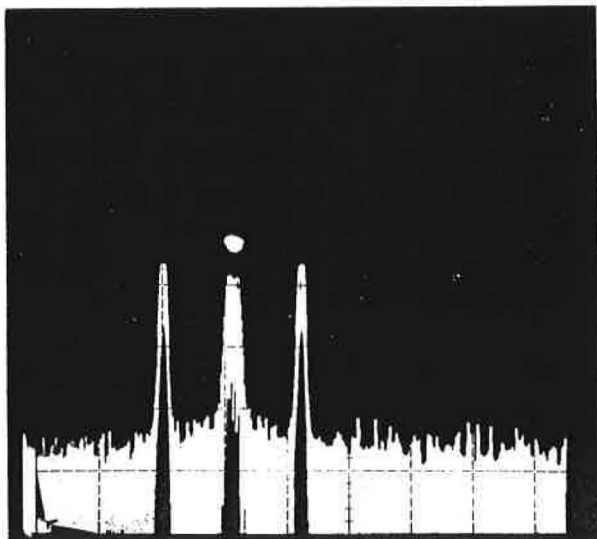


Fig.7-b. Photograph of spectrum analyser screen with 2,5 kHz/div. The modulation frequency was set to 2,8 kHz, a frequency which appears not to be in resonance with the eigenfrequencies of the pzt; only the centre frequency, indicated by a white dot and the modulation side bands are detected.

5.2 Beam Characteristics

5.2.1 Descriptive Laser Parameters

5.2.1.1 Formulas

Classical ray optics do not adequately describe the behaviour of laser beams. The beam profile is considered to be Gaussian. Five of the most common beam parameters [18] are illustrated in Fig.8: beam divergence (θ), the confocal parameter (b), beam waist (w_0), beam radius ($w(z)$) and radius of curvature ($R(z)$), where z indicates the distance in the beam direction, using the position of w_0 as origin.

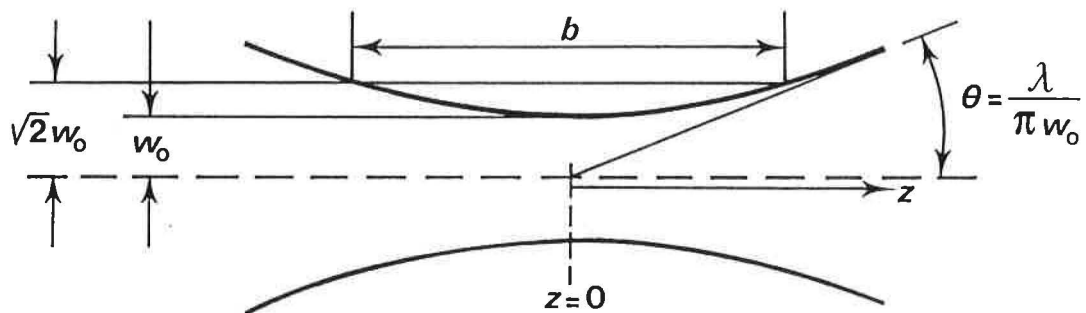


Fig.8. Schematized Gaussian beam parameters.

Analytically these parameters can be described as

$$\theta = \frac{\lambda}{\pi w_0} \quad (3-a)$$

$$b = \frac{2\pi w_0^2}{\lambda} \quad (3-b)$$

$$w(z) = w_0 \sqrt{1 + \frac{z^2 \lambda^2}{\pi^2 w_0^4}} \quad (3-c)$$

$$R(z) = z \left(1 + \frac{\pi^2 w_0^4}{\lambda^2 z^2} \right) \quad (3-d)$$

where λ represents the laser wavelength. Additionally, it is useful to know the value of the stability parameter g_i , which is defined as

$$g_i = 1 + \frac{L}{R_i} \quad (3-e)$$

where L represents the length of the laser cavity. For example, a resonator is defined to be stable when $0 < g_1 g_2 < 1$. It can further be shown that

$$w_0^2 = \frac{\lambda L}{\pi} \frac{\sqrt{(1 - g_1 g_2) g_1 g_2}}{(g_1 + g_2 - 2g_1 g_2)}, \quad (3-f)$$

see e.g. Shimoda [19]. Using a half symmetrical cavity, limited at one end by a mirror with the radius of curvature R and at the other by a flat mirror (or a grating) we obtain $g_1 = 1 - L/R$ and $g_2 = 1$, and it can hence be shown that

$$w_0^2 = \frac{\lambda}{\pi} \sqrt{L(R - L)}, \quad (3-g)$$

see e.g. [7]. Note that the stability condition is fulfilled for a half symmetrical cavity if $R > L$.

Finally, the Fresnel number N_F is familiar as

$$N_F = \frac{\Phi_T^2}{4\lambda L}, \quad (3-h)$$

where Φ_T is the free laser tube diameter. The diffraction loss is small if $N_F \gg 1$.

5.2.1.2 Parameters of the BIPM CO₂ Laser

Using the formalism presented in the previous section, the parameters of the laser are now calculated.

The radius of curvature, R , of the laser output mirror is $R=4$ m, and the distance, L , between the grating and the laser mirror is 1 m. Using (3-e), it is found that $g_1=1$ and $g_2=0,75$. w_0 can be calculated using (3-f) or (3-g) to give $w_0=2,42$ mm. This is the beam waist at the grating. The beam radius, w , is calculated to be 2,80 mm on the output mirror.

The angle of divergence is $\theta = 1,4$ mrad from (3-a). The value of N_F is found to be 1,9 for the laser tube, which indicates that the diffraction losses are reasonable.

Using a nomograph, Fahlen [20] has shown a useful way to deduce the beam parameters rapidly. Figure 9 is a nomograph showing the parameters for the current laser.

5.2.2 Beam Profile

After some manipulation of the position of the laser tube, a quasi-Gaussian intensity profile was found. The intensity distribution of the beam profile was measured using a 40 μm pinhole mounted on a translation device capable of moving in the horizontal and vertical directions. The output signal was measured with a HgCdTe detector. To improve the beam profile, the beam was passed through a spatial filter in the form of two convex lenses with focal lengths of 254 mm and a central pinhole of 600 μm diameter.

The result obtained by scanning in the horizontal direction through the vertical position at which the maximum intensity was found is displayed in Fig.10-a. The measured and fitted data are indicated by white and black squares respectively. The corresponding result obtained by scanning in the vertical direction is shown in Fig.10-b. The measured intensity is in arbitrary units (the maximum values are not identical in the two figures). This result is considered satisfactory.

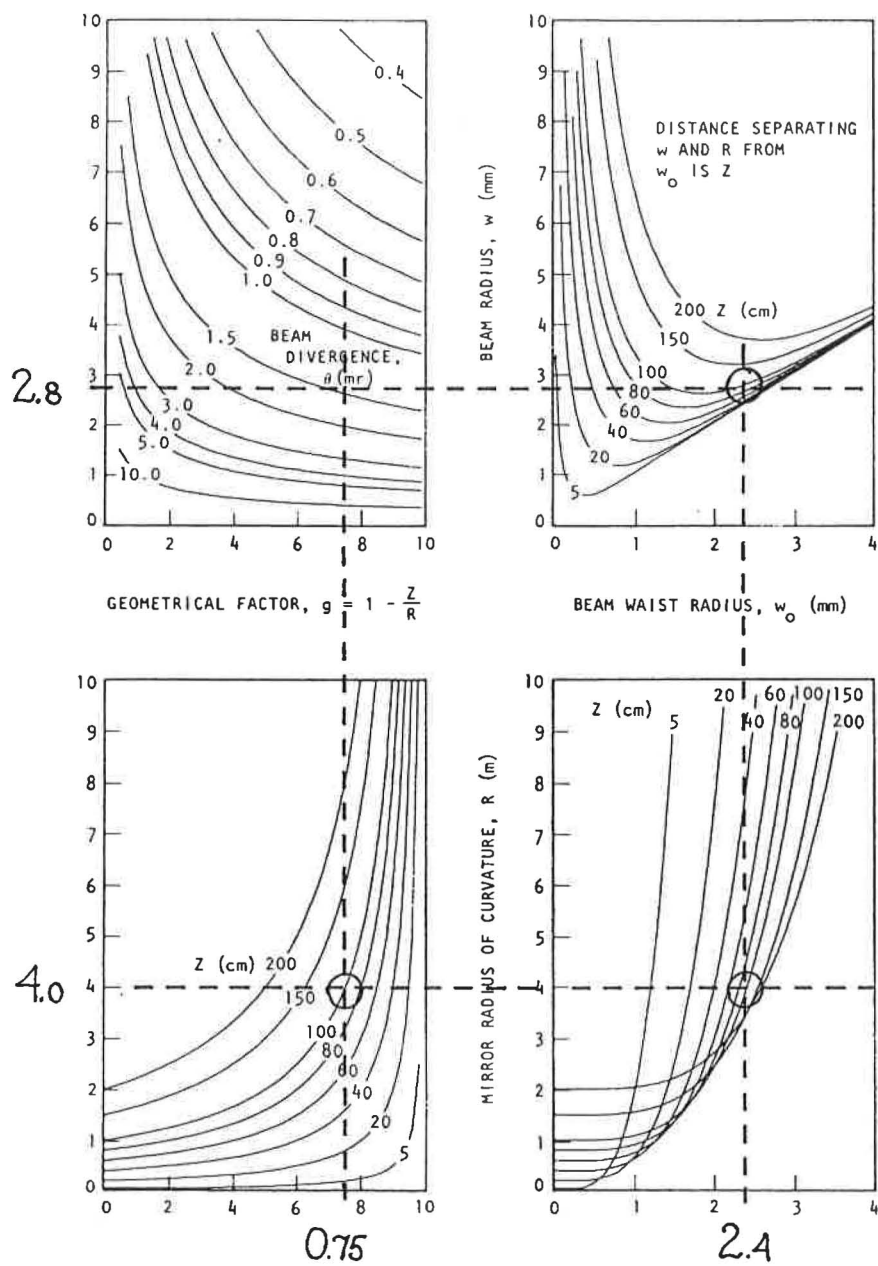


Fig.9. Extract from Fahlen [19] showing a nomograph with the geometrical beam parameters for our laser indicated by dashed lines.

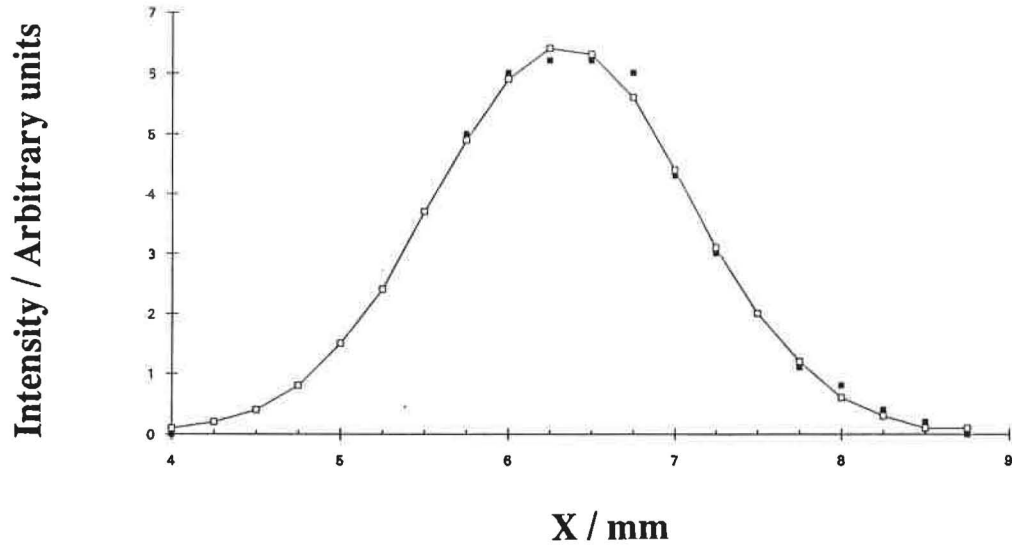


Fig.10-a. Measured intensity of the beam profile in arbitrary units, when scanning in the horizontal direction. The measured and fitted data are indicated by white and black squares respectively. The experimental data are joined by a solid line.

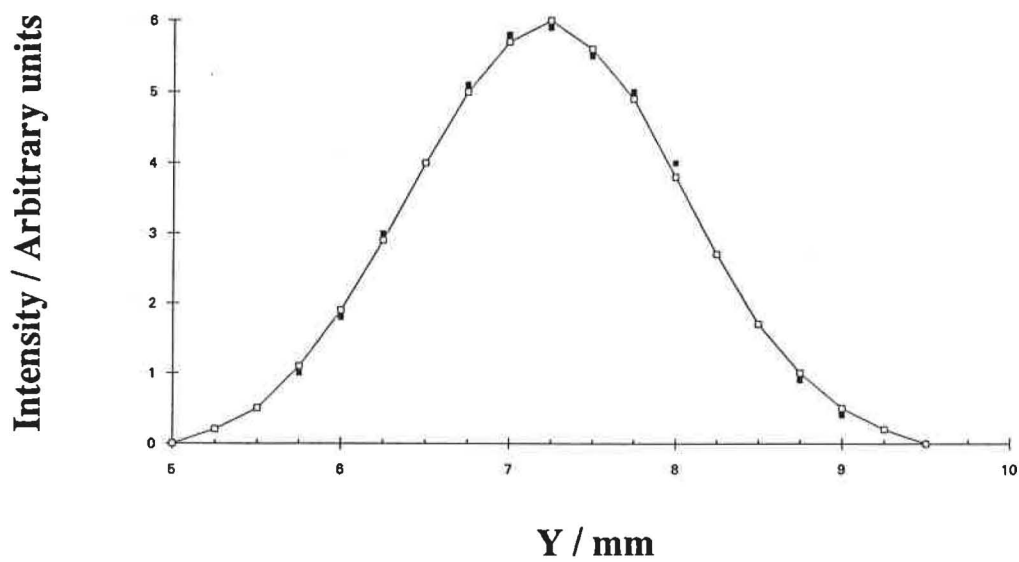


Fig.10-b. Measured intensity of the vertical beam profile in arbitrary units. The measured and fitted data are indicated by white and black squares respectively. The experimental data are joined by a solid line.

5.2.3 Pressure and Intensity

By optimizing the alignment of the laser tube the P(8)-P(32) and R(6)-R(22) laser lines were obtained, giving an intensity between 50 mW and 1,5 W at 1025 Pa (7.7 torr).

The laser mode is observed to increase in power at higher pressures as expected, see for example [21]. At very low pressures, fluorescing segments in the laser cavity between each anode-cathode pair can be observed. This phenomenon has been identified as moving striations and has been described by Wallard and Woods [22].

5.3 First Comparison

The opportunity occurred to compare the new BIPM CO₂ laser in free-running condition with one of the ETCA lasers, constructed by Dr Christian Bréant and his team. The BIPM laser (BC1) was compared with the ETCA laser (LUS1) by superposing the output beams and projecting them onto a liquid-nitrogen cooled HgCdTe detector. Both lasers were using the P(20) line of the 10 μm band. BC1 remained unstabilized, and LUS1 was frequency stabilized using SF₆ in an absorption cell.

Initially BC1 was secured mechanically without the elastic bearings, and on the first day a spectral purity of about 5 kHz was obtained. We obtained improved results the following two days by mounting the laser in its elastic bearings and fixing modelling clay to the metallic flexible tubes on each end of the laser (see Fig.4-a). With this configuration the spectrum shown in Fig.11-a was obtained. The full width at half maximum, indicated by the arrows in the figure, is 2,3 kHz, recorded during 0,6 seconds. This is narrow enough to allow satisfactory control of a stabilized laser system.

The Allan variance was also measured using the computerized measurement system at Dr Bréant's disposal. Figure 11-b illustrates the results obtained, where the estimated flicker floor is indicated by a straight horizontal line, around 350 Hz. This gives a relative frequency stability of 1,2 parts in 10¹¹.

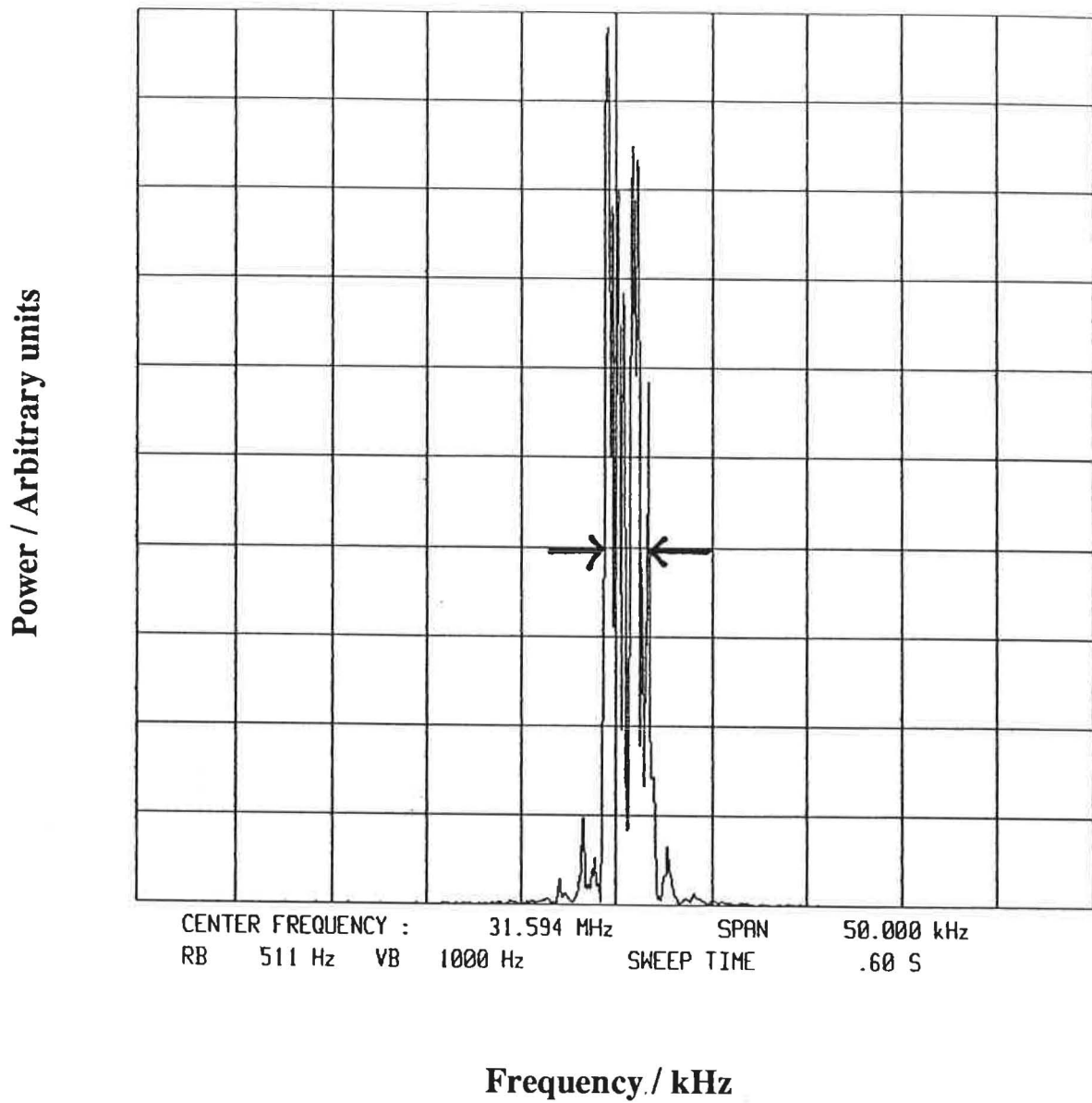


Fig.11-a. Measured frequency spectrum when comparing our laser in free run with the stabilized CO₂ laser of the ETCA. The spectral purity of the BIPM laser is 2,3 kHz.

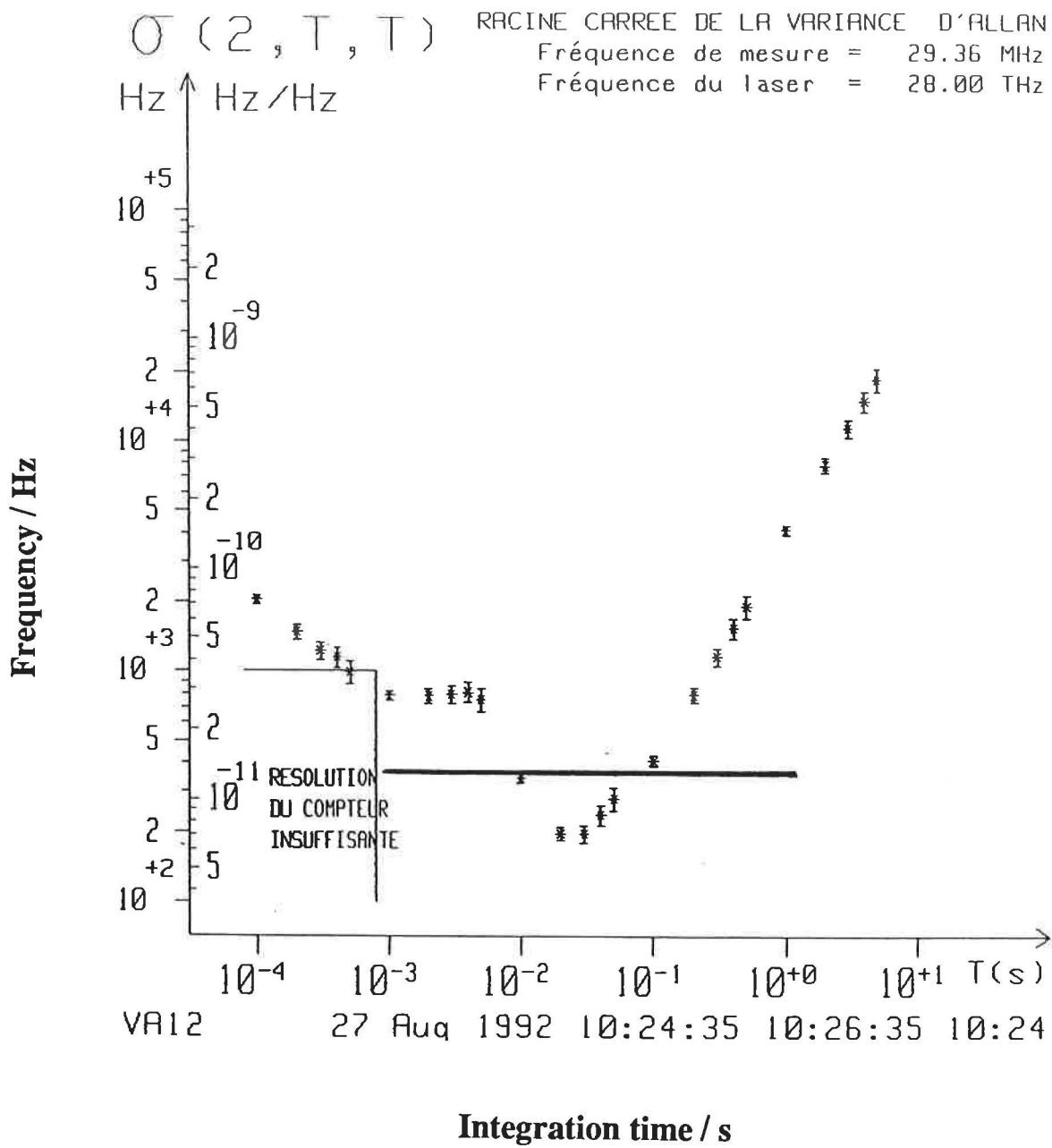


Fig.11-b. Measured Allan variance of the BIPM laser. The flicker floor level is estimated to be 350 Hz, corresponding to a relative stability of 1,2 parts in 10^{11} .

Acknowledgement

I wish to thank O. Acef (LPTF) for his hospitality, continuing support and for the many ideas originating in his laboratory. I also acknowledge the helpful comments by Ch. Bréant (ETCA) who made the laser comparison possible. The whole mechanical design was constructed by José Sanjaime and his competent group at the mechanical workshop at the BIPM, who have also given me encouraging discussions. I appreciate the help from numerous colleagues at the BIPM concerning vacuum problems, drawings and figures, ordering articles, various purchases, cleaning of cathode tubes, electric installations and other bits and pieces. I finally thank J.-M. Chartier for his advices, J. Labot for his disponibility and D.A. Blackburn and L. Robertsson for having criticized this manuscript.

References

- [1] C.K.N. Patel, Phys. Rev. Lett., 1964, **113**, 617-619.
- [2] N. Legay-Sommaire, L. Henry and F. Legay, C.R. Acad. Sc. Paris, 1965, **260**, 3339-3342.
- [3] Ch.J. Bordé, M. Ouhayoun, A. van Lerberghe, C. Salomon, S. Avrillier, C.D. Cantrell and J. Bordé, *Laser Spectroscopy IV*, Springer-Verlag, Berlin Heidelberg New York, 1979.
- [4] A. Clairon, B. Dahmani, A. Filimon and J. Rutman, IEEE Trans. Instr. Meas., 1985, **IM-34**, 265-268.
- [5] A. Clairon, O. Acef, C. Chardonnet and C.J. Bordé, *Frequency Standards and Metrology*, Springer-Verlag, Berlin Heidelberg, 1989.
- [6] O. Acef, J.J. Zondy, M. Abed, D.G. Rovera, A.H. Gérard, A. Clairon, Ph. Laurent, Y. Millerieux and P. Juncar, Opt. Commun., 1993, **97**, 29-34.
- [7] M. O. Acef, *Améliorations et comparaisons d'étalons de fréquences optiques. Développement d'un Spectromètre à très haute résolution autour de 28 THz et application à la spectroscopie de SF₆*. Thèse, Université de Paris-Sud 1989.
- [8] Ch. Bréant, private communication.
- [9] S. Fredin-Picard, *Sur la molécule diatomique*, Rapport BIPM-89/6.
- [10] G. Herzberg, *The Spectra and Structure of Simple Free Radicals An Introduction to Molecular Spectroscopy*, Cornell University Press, Ithaca and London, 1971.
- [11] G. Herzberg, *Spectra of Diatomic Molecules*, Van Nostrand Reinhold Company, New York, 1950.
- [12] L. C. Bradley, K. L. Soohoo and C. Freed, Absolute Frequencies of Lasing Transitions in Nine CO₂ Isotopic Species, IEEE J. Quantum Electron., 1986, **QE-22**, 234-267.
- [13] O. Svelto, *Principle of Lasers*, Plenum Press, New York London, 1976.
- [14] A. Clairon, private communication.
- [15] M. O. Acef, private communication.
- [16] J. Hecht, *The Laser Guidebook*, McGraw-Hill Book Company, New York, 1986.

- [17] R. Felder and L. Robertsson, *Results of the 1988 NRC absolute and relative frequency measurements carried out on portable (He-Ne)/CH₄ lasers*, Rapport BIPM-89/4.
- [18] H. Kogelnik and T. Li, *Laser Beams and Resonators*, Proc. IEEE, **54**, 1966, 1312-1329.
- [19] K. Shimoda, *Introduction to Laser Physics*, 2nd Ed, Springer-Verlag, Berlin Heidelberg New York, 1986.
- [20] T. S. Fahlen, *CO₂ Laser Design Procedure*, Appl. Opt., **12**, 1973, 2381-2390.
- [21] W.J. Witteman, *The CO₂ Laser*, Springer-Verlag, Berlin Heidelberg, 1987.
- [22] A.J. Wallard and P.T. Woods, Journ. Phys. E: Scient. Instr., **7**, 1974, 209-212.